A novel GPU-based sonar simulator for real-time applications

Rômulo Cerqueira[a,b], Tiago Trocoli[a], Gustavo Neves[a], Sylvain Joyeux[a], Jan Albiez[a,c], Luciano Oliveira[b]

[a]*Brazilian Institute of Robotics, SENAI CIMATEC, Salvador, Bahia, Brazil*
[b]*Intelligent Vision Research Lab, Federal University of Bahia, Salvador, Bahia, Brazil*
[c]*Robotics Innovation Center, DFKI GmbH, Bremen, Germany*

Abstract

Sonar simulation requires great computational effort, due to the complexity of acoustic physics related to the underwater environment. This fact turns the challenge of reproducing sensor data into a non-trivial task. On the other hand, simulation of sonar data makes algorithms and control system evaluations avoid the presence of real underwater environment; that reduces the cost and risks in field experiments, specially involving underwater robotics domain. This paper proposes a novel underwater imaging sonar simulator, which relies on OpenGL shading language (GLSL) chain. The virtual underwater scene is built on three frameworks: (i) OpenSceneGraph (OSG) reproduces the ocean visual effects, (ii) Gazebo deals with physics effects, and (iii) robot construction kit (Rock) lets control the sonar on underwater environment. Our sonar simulation returns a matrix comprised of the echo intensity, the distance to the target object and angle distortion information, being calculated on object shapes and material properties in the 3D rendered scene. Sonar-based speckle noise and object material properties are also considered as the part of the sonar image. Our evaluation demonstrated that the proposed method is able to operate with high frame rate, as well as realistic sonar image quality in different virtual underwater scenarios.

Key words: Synthetic sensor data, sonar imaging, GPU-based processing, robot construction kit, Underwater robotics.

1. Introduction

Simulation is an useful tool for designing and programming autonomous robot systems. That allows evaluating robot behavior, without the physical hardware, or algorithms and control systems in real-time trials, without the need to run costly experiments. Real-time applications usually require simulation platforms for rapid prototyping in order to reproduce realistic environments and sensors, with the goal of testing decision making algorithms in dynamic domains.

Autonomous underwater vehicles (AUVs) usually demand expensive hardware and a restrictive operational environment. Due to environment constraints, which avoid the AUV communicating with ground station via a totally reliable acoustic link, the robot must be able to make completely autonomous decisions. While the analysis and interpretation of sensor data can be thoroughly tested on recorded data, for testing and evaluation of vehicle's motion responses for this data, a simulation is needed to tuning control parameters and avoid involved risks on real world drives.

Since AUVs act below the photic zone, with high turbidity and huge light scattering, image acquisition by optical devices is limited by short ranges and clear visibility conditions. To tackle that limitations, high-frequency sonars have been used on AUVs' perception system rather than optical devices for underwater applications.

Acoustic waves emitted by sonars are significantly less affected by water attenuation, facilitating operation at greater ranges even as low-to-zero visibility conditions, with a fast refresh rate. Sonar devices usually solve the main shortcomings of optical sensors at the expense of providing noisy data of lower resolution and more difficult interpretation.

In the FlatFish project [1] was developed an interface to integrate the Gazebo real-time simulator [1] into the software framework ROCK [2] as presented in [2]. With this integration it is able to simulate basic underwater physics and underwater camera systems. The missing part, needed by most underwater robots, was the sonar system.

1.1. Related work

Recent works proposed ray tracing- and tube tracing-based techniques to simulate sonar data with very accurate results, but at a high computational cost [3, 4, 5, 6, 7, 8, 9]. Bell and Linett [3] proposed a simulator using optical ray tracing for underwater side-scan sonar imagery; images were generated by the use of acoustic signals represented by rays, which are repeatedly processed forming a 2D-array, representing all angles that the sonar can emit signal. Waite [4] used of frequency-domain signal processing to generate synthetic aperture sonar frames. In this method, the acoustic image was created by expressing the Fourier transform of the acoustic pulse used to insonifying the scene.

---

[1]http://gazebosim.org
[2]http://rock-robotics.org/

For foward-looking sonar simulations, Saç *et al* [5] described the sonar model by computing the ray tracing in frequency domain. When a ray hits an object in 3D space, three parameters are calculated to process the acoustic data: the euclidean distance from the sonar axis, the intensity of returned signal by Lambert Illumination model and the surface normal. The reverberation and shadow phenomena are also addressed. In De-Marco *et al* [6], the rays are used in Gazebo and ROS [3](Robot Operating System) integration to simulate the acoustic pulse and produce a 3D point cloud of covered area. Since the material reflectivity was statically defined, it resulted in the same intensity values for all points on a single object. Gu *et al* [7] modeled a FLS device where the ultrasound beams were formed by a set of rays. However, the acoustic image is significantly limited by its representation by only two colors: white, when the ray strike an object, and black for shadow areas. This approach was evolved by Kwak et al [8] by adding a sound pressure attenuation to produce the gray-scale sonar frame, while the other physical characteristics related to sound transmission are disregarded.

1.2. Contributions

This paper presents a computationally efficient sonar simulator which manipulates the rendering pipeline to compute a sonar image by two kind of imaging sonar devices.

The proposed approach herein entails several novelties. As opposed to the related works, the depth and normal values are directly manipulated during the scene formation, which generate sonar frames with a low computational cost and allow the usage by real-time applications. Also, this method is able to reproduce any type of underwater sonar images, as seen in evaluation tests with two kind of sonar devices.

In addition to our previous work [9], the normal data can also be defined by bump mapping technique and material's reflectivity. Moreover, the speckle noise is modeled as a non-uniform Gaussian distribution and added to final sonar image.

2. Sonar operation

2.1. Sonar image model

Sonars are echo-ranging devices that use acoustic energy to locate and survey objects in a desired underwater area. The sonar transducer emits pulses of sound waves (or ping) until they hit with any object or be completely absorbed. When the acoustic signal collides with a surface, part of this energy is reflected, while other is refracted. Then the sonar data is built by plotting the echo measured back versus time of acoustic signal.

A single beam transmitted from a sonar is seen in Fig. 1. The horizontal and vertical beamwidths are represented by the azimuth ψ and elevation θ angles respectively, where each sampling along the beam is named *bin*. The x-axis is perpendicular to the sonar array, the y-axis is to the right, z-axis points down and the covered area is defined by r_{min} and r_{max}. Since the speed of sound underwater is known or can be measured, the time delay between the emitted pulses and their echoes reveals how far the objects are (distance r) and how fast they are moving. The backscattered acoustic power in each bin determines the intensity value.

The array of transducer readings, with different azimuth directions, forms the final sonar image. Since all incoming signals converge on the same point, the reflected echoes could have originated anywhere along the corresponding elevation arc at a fixed range, as seen in Fig. 1. Therefore, the 3D information is lost in the projection into a 2D image [10].
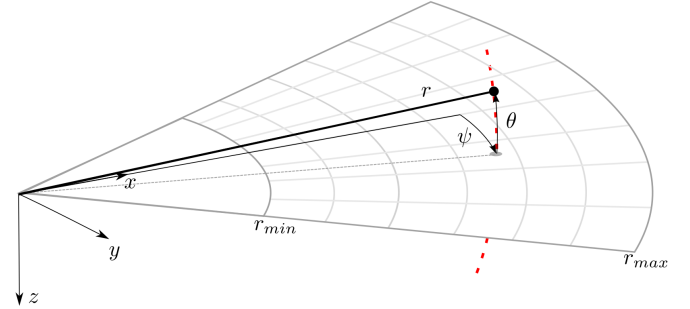

Figure 1: Imaging sonar geometry [10]. By the projection process, all 3D points belong the same elevation arc (represented as dashed red line) will be represented to the same image point in the 2D plane. So the range r and the azimuth angle ψ are measured, however the elevation angle θ is lost.

2.2. Sonar characteristics

Although the sonar devices address the main shortcomings of optical sensors, they present more difficult data interpretation, such as:

(a) Shadowing: This effect is caused by objects blocking the sound waves transmission and causing regions behind them without acoustic feedback. These regions are defined by a black spot in the image occluding part of the scene;

(b) Non-uniform resolution: The amount of pixels used to represent an intensity record grow as its range increases. This fact causes image distortions and object flatness;

(c) Changes in viewpoint: Imaging the same scene from different viewpoints can cause occlusions, shadows movements and significant alterations of observable objects [11]. For instance, when an outstanding object is insonified, its shadow gets shortened as the sonar becomes closer;

(d) Low SNR (Signal-to-Noise Ratio): The sonar suffers from low SNR mainly due the very-long-range scanning and the presence of speckle noise introduced caused by acoustic wave interferences [12].

2.3. Types of underwater sonar devices

The most common types of acoustic sonars are mechanical scanning imaging sonar (MSIS) and forward-looking sonar (FLS). In the first one (Fig. 2(a)), with one beam per reading, the sonar image is built for each pulse; these images are usually shown on a display pulse by pulse, and the head position reader

is rotated according to motor step angle. After a full 360° sector reading (or the desired sector defined by left and right limit angles), the accumulated sonar data is overwritten. In contrast, the acquisition of a scan image involves a relatively long time and introduces distortions by vehicle movement. This sonar device is useful for obstacle avoidance [13] and navigation [14] applications.

For the FLS, as seen in Fig. 2(b), with *n* beams being read simultaneously, the whole forward view is scanned and the current data is overwritten by the next one with a high framerate, similar to a streaming video imagery for real-time applications. This imaging sonar is commonly used for navigation [15], mosaicing [11], target tracking [16] and 3D reconstruction [10] approaches.
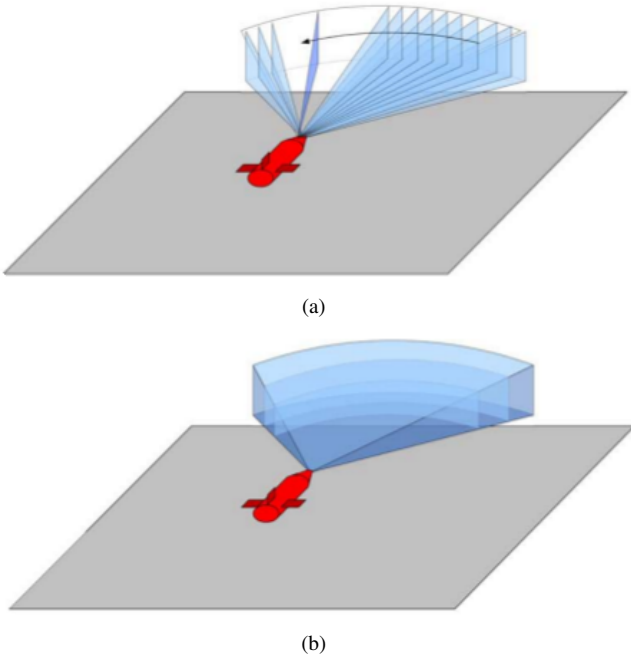

(a)

(b)

Figure 2: Different underwater sonar readings: Mechanically Scanning Imaging Sonar (a) and Forward-Looking Sonar (b).

3. GPU-based sonar simulation

The goal of this work is to simulate any kind of underwater sonar by vertex and fragment processing, with a low computational cost. The complete pipeline of this implementation, from the virtual scene to the synthetic acoustic image, is seen in Fig. 3 and is detailed in the following subsections. The sonar simulation is written in C++ with OpenCV [4] support as Rock packages.

3.1. Rendering underwater scene

The Rock-Gazebo integration [2] provides the underwater scenario and allows real-time Hardware-in-the-Loop simulations, where Gazebo handles the physical engines and the Rock's

visualization tools are responsible by the scene rendering. The graphical data in Rock are based on OpenSceneGraph [5] library, an open source C/C++ 3D graphics toolkit built on OpenGL. The osgOcean [6] library is used to simulate the ocean's visual effects, and the ocean buoyancy is defined by the Gazebo plugin as described in Watanabe et al [2].

All scene's aspects, such as world model, robot parts (including sensors and joints) and others objects presented in the environment are defined by SDF files, which uses the SDFormat [7], a XML format used to describe simulated models and environments for Gazebo. Also, the vehicle and sensor robot description must contain a geometry file. Visual geometries used by the rendering engine are provided in COLLADA format and the collision geometries in STL data.

Each component described in the SDF file becomes a Rock component, which is based on the Orocos RTT (Real Time Toolkit) [8] and provides ports, properties and operations as its communication layer. When the models are loaded, Rock-Gazebo creates ports to allow other system components to interact with the simulated models [9]. A resulting scene sample of this integration is seen in Fig. 4.

3.2. Shader rendering

Modern graphics hardware presents programmable tasks embedded in GPU. Based on parallel computing, this approach can speed up 3D graphics processing and reduce the computational effort of Central Processing Unit (CPU).

The rendering pipeline can be customized by defining programs on GPU called shaders. A shader is written in OpenGL Shading Language (GLSL) [9], a high-level language with a C-based syntax which enables more direct control of graphics pipeline avoiding the usage of low-level or hardware-specific languages. Shaders can describe the characteristics of either a vertex or a fragment (a single pixel). Vertex shaders are responsible by transform the vertex position into a screen position by the rasterizer, generating texture coordinates for texturing, and lighting the vertex to determine its color. The rasterization results in a set of pixels to be processed by fragment shaders, which manipulate their locations, depth and alpha values and interpolated parameters from the previous stages, such as colors and textures [17].

In this work, the underwater scene is sampled by a virtual camera, whose optical axis is aligned with the intended viewing direction of the imaging sonar, as well as the covered range and opening angle. By programming the fragment and vertex shaders, the sonar data is computed as:

(a) *Depth* is the camera focal length and is calculated by the euclidean distance to object's surface point;

(a) *Intensity* presents the echo reflection energy based on object's surface normal angle to the camera;

---

[4]http://opencv.org/

[5]http://www.openscenegraph.org/

[6]http://wiki.ros.org/osgOcean

[7]http://sdformat.org

[8]http://www.orocos.org/rtt

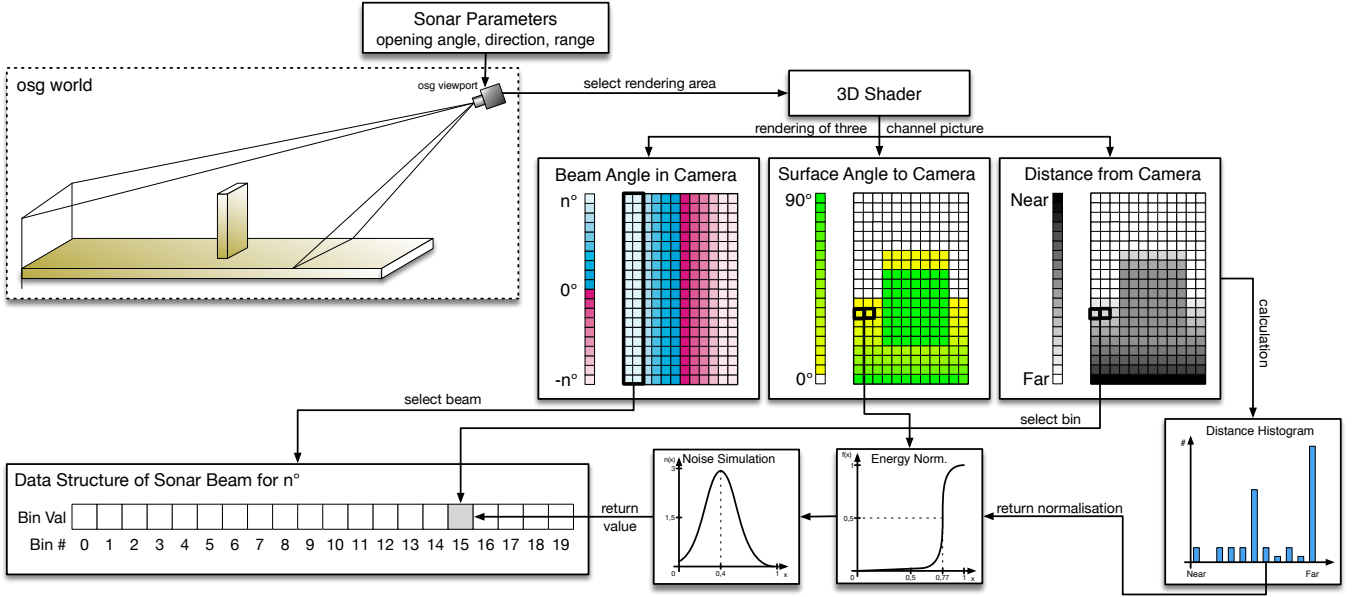[9]https://www.opengl.org/documentation/glsl/

Figure 3: A graphical representation of the individual steps to get from the OpenSceneGraph scene to a sonar beam data structure.
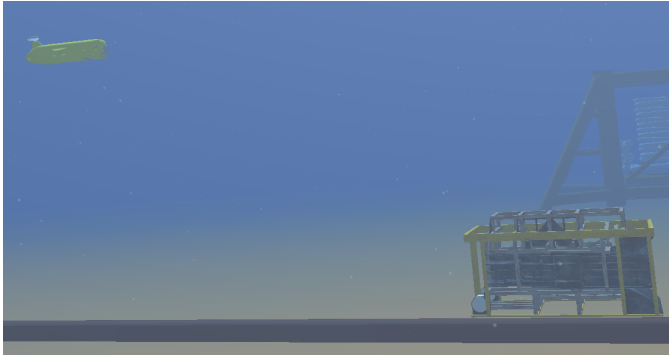

Figure 4: FlatFish AUV in ROCK-Gazebo underwater scene.

(a) *Angular distortion* is the angle formed from the camera center column to the camera boundary column, for both directions.

These data are normalized in [0,1] interval, where means no energy and maximum echo energy for intensity data respectively. For depth data, the minimum value portrays a close object while the maximum value represents a far one, limited by the sonar maximum range. Angle distortion value is zero in image center column which increases for both borders to present the half value of horizontal field of view.

Most real-world surfaces present irregularities and different reflectances. For more realistic sensing, the normal data can also be defined by bump mapping and material properties. Bump mapping is a perturbation rendering technique to simulate wrinkles on the object's surface by passing textures and modifying the normal directions on shaders. It is much faster and consumes less resources for the same level of detail compared to displacement mapping, because the geometry remains unchanged. Since bump maps are built in tangent space, in-terpolating the normal vertex and the texture, a TBN (Tangent, Bitangent and Normal) matrix is computed to convert the normal values to world space. The different scenes representation is seen in Fig. 5.

Moreover, the reflectance allows to describe properly the intensity back from observable objects in shader processing according their material properties (e.g. aluminium has more reflectance than wood and plastic). When an object has its reflectivity defined, the reflectance value R is passed to fragment shader and must be positive. As seen in Fig. 6, when the normal values are directly proportional to the reflectance value R.

At the end, the shader process gives a 3-channel matrix data of intensity, depth and angular distortion stored in each channel.

3.3. Simulating sonar device

The 3D shader matrix is processed in order to build the corresponding acoustic representation. Since the angular distortion is radially spaced over the horizontal field of view, where all pixels in the same column have the same angle value, the first step is to split the image in number of beam parts. Each column is correlated with its respective beam, according to sonar bearings, as seen in Fig. 3.

Each beam subimage is converted into bin intensities using the depth and intensity channels. In a real imaging sonar, the echo measured back is sampled over time and the bin number is proportional to sensor's range. In other words, the initial bins represent the closest distances, while the latest bins are the furthest ones. Therefore, a distance histogram is evaluated to group the subimage pixels with their respective bins, according to depth channel. This information is used to calculate the accumulated intensity of each bin.

Due to acoustic beam spreading and absorption in the water, the final bins have less echo strength than the first ones,
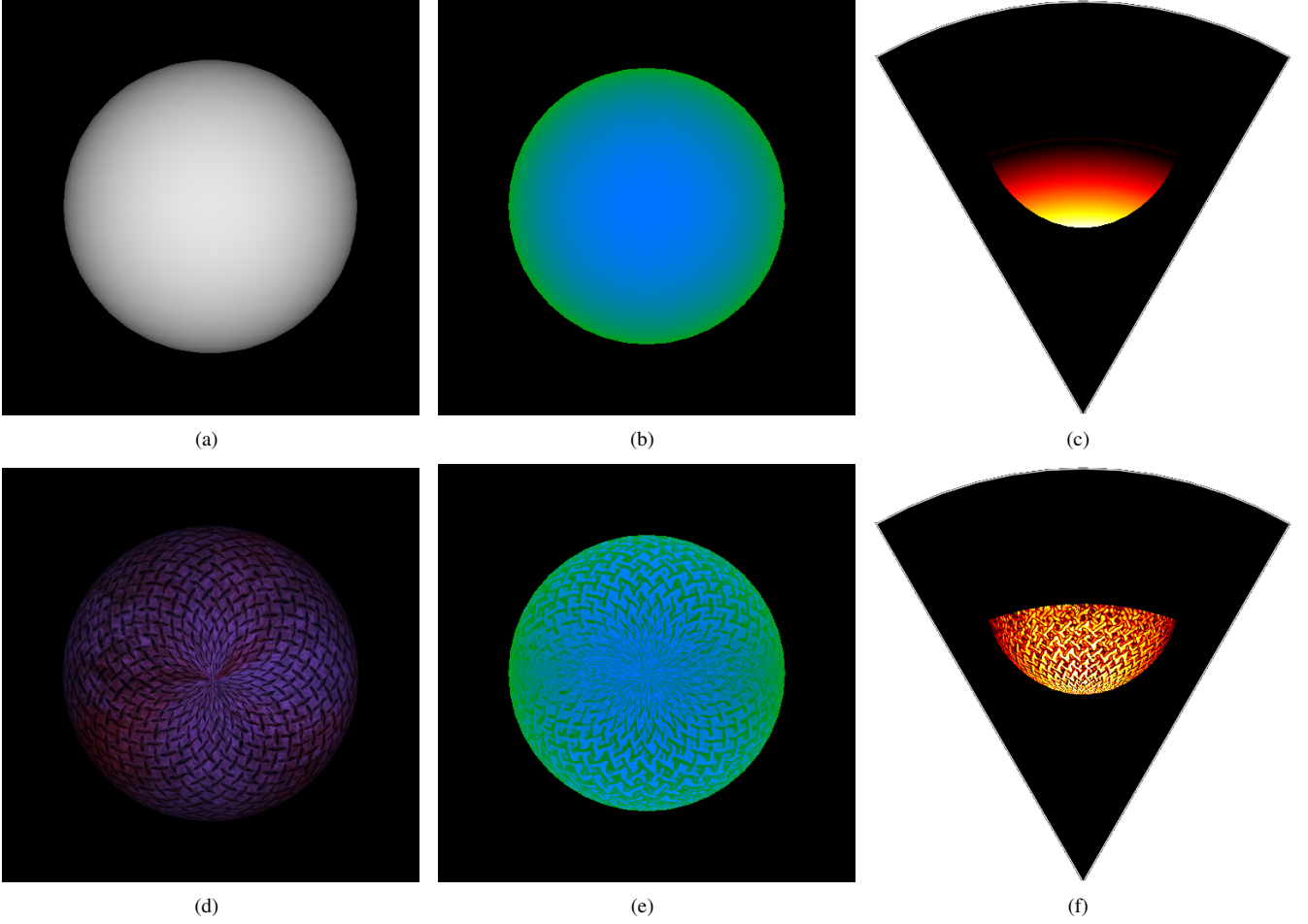
4

Figure 5: Shader rendering with bump mapping processing example: sphere without texture (a) and with texture (d); their respective shader image representation in (b) and (e), where the blue is the normal channel and green is the depth one; and the final acoustic image in (c) and (f). By bump mapping technique, the texture changes the normal directions and the sonar image are more realistic in comparison to real objects appearances.

because the energy is lost two-way in the environment. In order to solve this, the sonar devices use a energy normalization based on time-varying gain for range dependence compensation which spread losses in the bins [18]. In this simulation approach, the accumulated intensity in each bin is normalized as

$$I_{bin} = \sum_{x=1}^{N} \frac{1}{N} \times S(i_x), \qquad (1)$$

where I_{bin} is the intensity in the bin after the energy normalization, x is the pixel in the shader matrix, N is the depth histogram value (number of pixels) of that bin, $S(i_x)$ is the sigmoid function and i_x is the intensity value of the pixel x.

Finally, the sonar image resolution needs to be big enough to fill all bins informations. In this case, the number of bins involved is in direct proportion to the sonar image resolution.

3.4. Noise model

Imaging sonar systems are perturbed by a multiplicative noise known as speckle. It is caused by coherent processing of backscattered signals from multiple distributed targets, that degrades image quality and the visual evaluation. Speckle noise results in constructive and destructive interferences which are shown as bright and dark dots in the image. The noisy image has been expressed as [19]:

$$y(t) = x(t) \times n(t), \qquad (2)$$

where t is the time instant, $y(t)$ is the noised image, $x(t)$ is the free-noise image and $n(t)$ is the speckle noise matrix.

This kind of noise is well-modeled as a Gaussian distribution. The physical explanation is provided by the Central Limit of Theorem, which states that the sum of many independent and identically distributed random variables tends to behave a Gaussian random variable [20].

A Gaussian distribution is built following a non-uniform distribution, skewed towards low values, as seen in Fig. 3, and applied as speckle noise in the simulated sonar image. After that, the simulation sonar data process is done.

3.5. Integrating sonar device with ROCK

To export and display the sonar image, the simulated data is encapsulated as Rock's sonar data type and provided as an
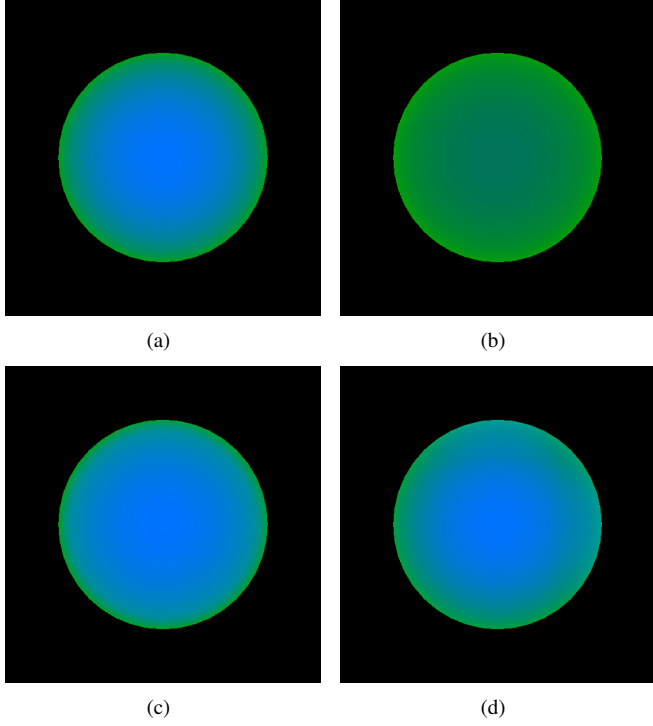
Figure 6: Examples of different reflectance values *R* on shader image representation, where blue is the normal channel and green is the depth channel: raw image (a); *R* = 0.35 (b); *R* = 1.40 (c); and *R* = 2.12 (d).

output port of Rock's component.

4. Simulation results and experimental analysis

For the evaluation of the proposed simulator, the experiments were conducted by using a 3D model of FlatFish AUV equipped with two MSIS and one FLS sensors on different scenarios. The MSIS sensors are located in AUV's top and back and they are configured as follows: opening angle of 3° by 35°, 500 bins in the single beam, a full 360° sector scan reading and a motor step of 1.8°. By other hand, the FLS takes place in AUV's bottom with the following set: field of view of 120° by 20°, 256 beams simultaneously, 1000 bins per each beam and angle tilt between the sonar and AUV of 20°. While the scene's frames were captured by the sonars, we sequentially present the resulting simulated acoustic images.

4.1. Experimental evaluation

The virtual FLS from FlatFish AUV was used to insonify scenes in three scenarios. A docking station, in parallel with a pipeline on the seabed, composes the first scenario, as seen in Fig. 7(a). The target's surface is well-defined in the simulated acoustic frame, as seen in Fig. 7(b), even as the shadows and speckle noise. Given the docking station is metal-made, the texture and reflectivity were set, resulting in a higher intensity shape in comparison with the other targets.

The second scenario presents the vehicle in front of a manifold model on a non-uniform seabed, as seen in Fig. 7(c). The target model was insonified to generate the sonar frame from the underwater scene. The frontal face of the target, as well the portion of the seabed and the degraded data by noise, are clearly visible in the FLS image. Also, a long acoustic shadow is formed behind the manifold, occluding part of the scene.

The third scenario contains a SSIV (SubSea Isolation Valve) structure connected with a pipeline in the bottom, presented in Fig. 7(e). The targets' shapes are well-defined, such as their shadows.

Due the sensor configuration and the robot position, the initial bins usually present a blind region in the three simulated scenes, caused by absence of objects at lower ranges, similar with real images. Also, the brightness of seafloor decreases when it makes farthest from sonar due the normal orientation of surface.

The MSIS sensor was also simulated in three different experiments. The FlatFish robot in a big textured tank composed the first scene, as seen in Fig. 8(a). Even as the first scenario of FLS experiment, the reflectivity and texture were set to the target. The rotation of frontal sonar head position, by a complete 360° scanning, produced the acoustic frame of tank walls, seen in Fig. 8(b).

The second experiment involves the vehicle's movement during the data acquisition process. The scene contains a grid around the AUV, as seen in Fig. 8(c), and the frontal MSIS is used. This trial induces a distortion in the final acoustic frame, because the relative sensor's position with respect to surrounding object changes while the sonar image is being built, as seen in Fig. 8(d). In this case, the robot rotates 20° left during the scanning.

The last scenario presents the AUV over oil and gas structures on the sea bottom, as seen in Fig. 8(e). Using the back MSIS, with a vertical orientation, the scene was scanned in order to produce the acoustic visualization. As seen in Fig. 8(f), the objects' surfaces present clear definition in the small scanning section of the seafloor.

4.2. Computational time

The performance evaluation for this approach was determined as part of suitable analysis for real-time applications. The experiments were performed on a personal computer with Ubuntu 16.04 64 bits, Intel Core i7 3540M processor running at 3 GHz with 16GB DDR3 RAM memory and NVIDIA NVS 5200M video card.

The elapsed time of each sonar data is stored to compute the mean and standard deviation metrics, after 500 iterations, as presented in Tables 1 and 2. After changing the device parameters, such as number of bins, number of beams and field of view, the proposed approach generated the sonar frames with a high frame rate, for both sonar types. Given the Tritech Gemini 720i, a real forward-looking sonar sensor with a field of view of 120° by 20° and 256 beams presents a maximum update rate of 15 frames per second, the results grant the usage of the sonar simulator for real-time applications. Also, the MSIS data built by the simulator is able to complete a 360° scan sufficiently time short in comparison with a real sonar as Tritech Micron DST.
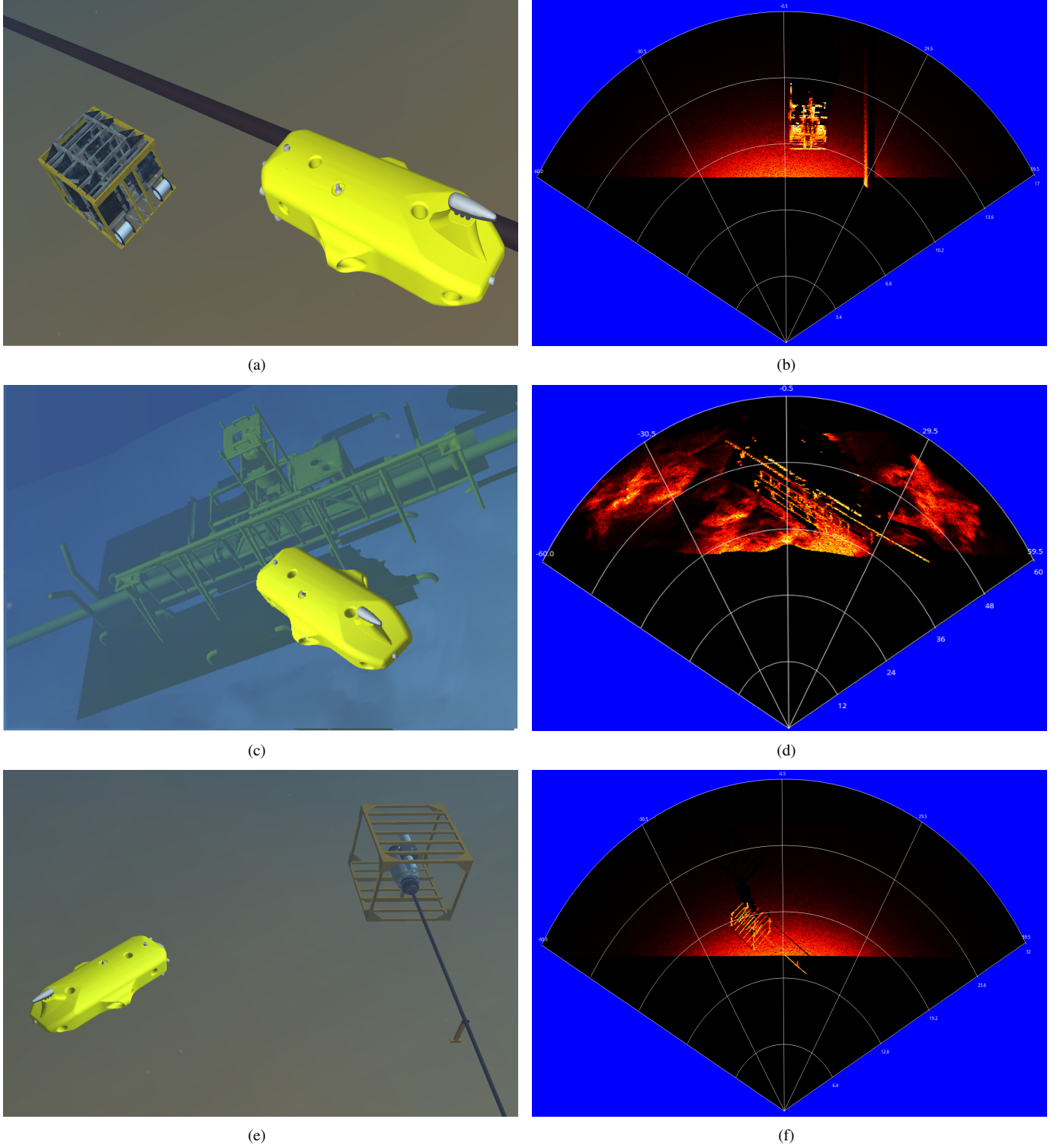
6

Figure 7: Forward-looking sonar simulation experiments: (a), (c) and (e) present the virtual underwater trials, while (b), (d) and (f) are the following acoustic representations of each scenario, respectively.

Moreover, since the number of bins is directly proportional to sonar image resolution, as explained in Section 3.3, this is also correlated with the computation time. When the number of bins increases, the simulator will have a bigger scene frame to compute and generate the sonar data.
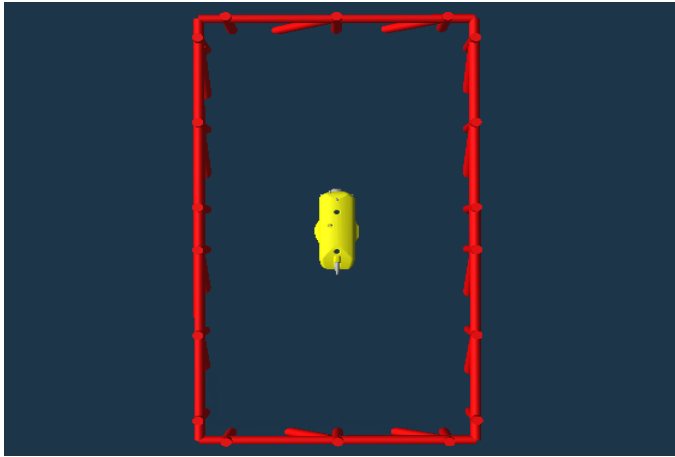
5. Conclusion and future work

We presented a GPU-based approach for imaging sonar simulation. By the evaluation results on different scenarios, the targets were well-defined on simulated sonar frames. The same
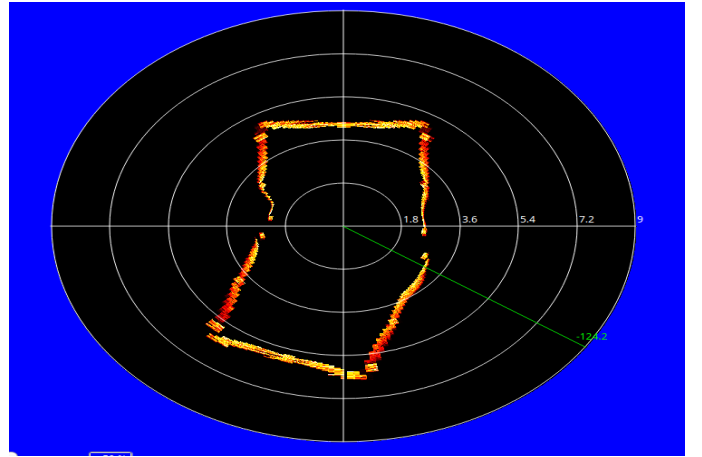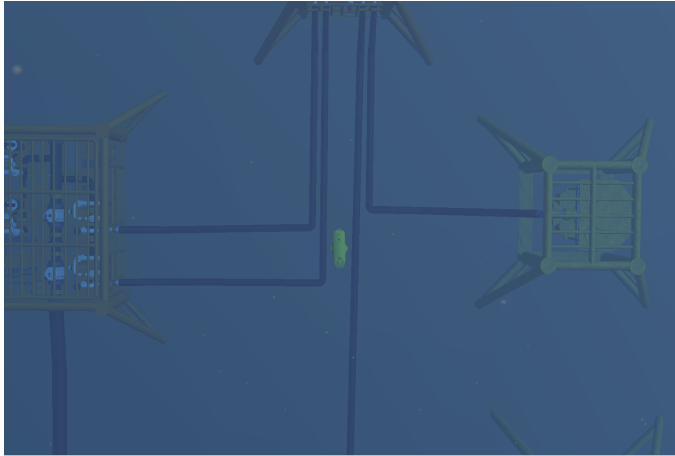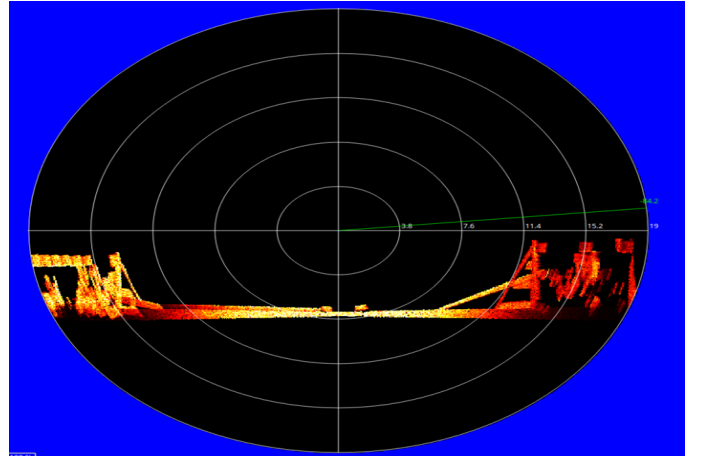
7
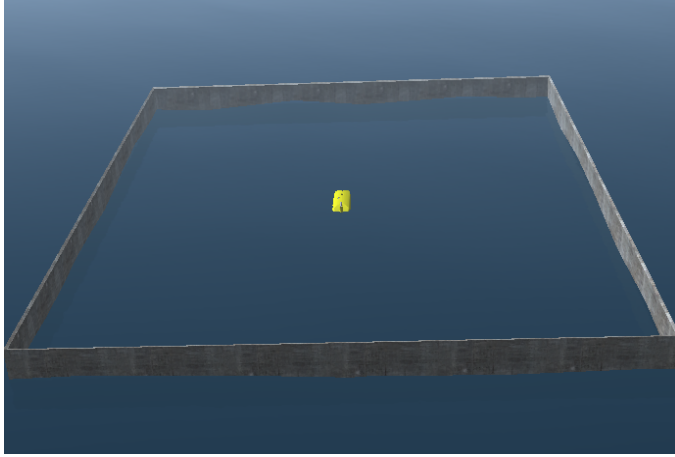
(a)
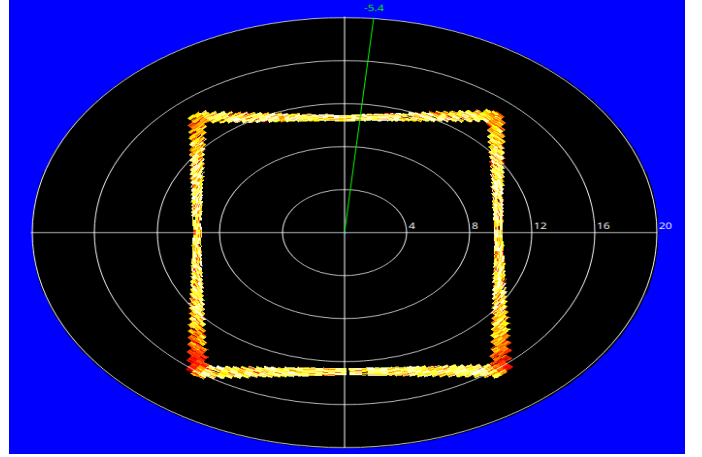
(b)

(c)

(d)

(e)

(f)

Figure 8: Mechanical Scanning Imaging Sonar experiments: the underwater scenes presented (a), (c) and (e) and the following simulated frames in (b), (d) and (f), respectively.

model was able to reproduce the sensoring of two kind of sonar devices (FLS and MSIS). Moreover, the real sonar image singularities, such as speckle noise, surface irregularities, shadows, material properties and shapes are also addressed and represented on the synthetic acoustic images.

In addition, the processing time was calculated with different sonar parameters (field of view, number of bins and number of beams). The vertex and fragment processing during the underwater scene rendering accelerates the sonar image building and the mean and standard deviation metrics certified the per-

Table 1: Processing time to generate FLS frames with different parameters.

# of samples	# of beams	# of bins	Field of view	Average time (*ms*)	Std dev (*ms*)	Frame rate (*f ps*)
500	128	500	120° x 20°	54.7	3.7	18.3
500	128	1000	120° x 20°	72.3	8.9	13.8
500	256	500	120° x 20°	198.7	17.1	5.0
500	256	1000	120° x 20°	218.2	11.9	4.6
500	128	500	90° x 15°	77.4	11.8	12.9
500	128	1000	90° x 15°	94.6	10.2	10.6
500	256	500	90° x 15°	260.8	18.5	3.8
500	256	1000	90° x 15°	268.7	16.7	3.7

Table 2: Processing time to generate MSIS samples with different parameters.

# of samples	# of bins	Field of view	Average time (*ms*)	Std dev (*ms*)	Frame rate (*f ps*)
500	500	3° x 35°	8.8	0.7	113.4
500	1000	3° x 35°	34.5	1.6	29.0
500	500	2° x 20°	10.3	0.6	96.7
500	1000	2° x 20°	41.7	3.7	24.0

formance is much closely to real imaging sonars. Therefore, the results granted the usage of this imaging sonar simulator by real-time applications, such as target tracking, obstacle avoidance and localization and mapping algorithms.

Next steps will focus on qualitative and computation-efficiency evaluations with other imaging sonar simulators.

References

[1] Albiez J, Joyeux S, Gaudig C, Hilljegerdes J, Kroffke S, Schoo C, et al. FlatFish - a compact AUV for subsea resident inspection tasks. In: MTS/IEEE OCEANS Conference. 2015, p. 1–8.

[2] Watanabe T, Neves G, Cerqueira R, Trocoli T, Reis M, Joyeux S, et al. The Rock-Gazebo integration and a real-time AUV simulation. In: IEEE Latin American Robotics Symposium (LARS). 2015, p. 132–8.

[3] Bell JM, Linnett LM. Simulation and analysis of synthetic sides-can sonar images. In: IEEE Radar, Sonar and Navigation Conference. 1997, p. 219–26.

[4] Wait AD. Sonar for practising engineers. Wiley; 2002.

[5] Saç H, Leblebicioğlu K, Bozdaği Akar G. 2d high-frequency forward-looking sonar simulator based on continuous surfaces approach. Turkish Journal of Electrical Engineering and Computer Sciences 2015;23(1):2289–303.

[6] DeMarco K, West M, Howard A. A computationally-efficient 2d imaging sonar model for underwater robotics simulations in Gazebo. In: MTS/IEEE OCEANS Conference. 2015, p. 1–8.

[7] Gu J, Joe H, Yu SC. Development of image sonar simulator for underwater object recognition. In: MTS/IEEE OCEANS Conference. 2013, p. 1–6.

[8] Kwak S, Ji Y, Yamashita A, Asama H. Development of acoustic camera-imaging simulator based on novel model. In: IEEE International Conference on Environment and Electrical Engineering (EEEIC). 2015, p. 1719–24.

[9] Cerqueira R, Trocoli T, Neves G, Oliveira L, Joyeux S, Albiez J. Custom shader and 3d rendering for computationally efficient sonar simulation. In: Workshop on Work in Progress, held at Conference on Graphics, Patterns and Images (SIBGRAPI). 2016, p. 1–5.

[10] Huang TA, Kaess M. Towards acoustic structure from motion for imaging sonar. In: IEEE/RSJ International Conference on Intelligent Robots and Systems (IROS). 2015, p. 758–65.

[11] Hurtós N. Forwad-looking sonar mosaicing for underwater environments. Ph.D. thesis; Universitat de Girona; 2014.

[12] Abbot J, Thurstone F. Acoustic speckle: theory and experimental analysis. Ultrasonic Imaging 1979;1(4):303–24.

[13] Ganesan V, Chitre M, Brekke E. Robust underwater obstacle detection and collision avoidance. Autonomous Robots 2015;40(7):1–21.

[14] Ribas D, Ridao P, Neira J. Underwater SLAM for structured environments using an imaging sonar. Springer-Verlag Berlin Heidelberg; 2010.

[15] Fallon MF, Folkesson J, McClelland H, Leonard JJ. Relocating underwater features autonomously using sonar-based SLAM. Journal of Ocean Engineering 2013;38(3):500–13.

[16] Liu L, Xu W, Bian H. A LBF-associated contour tracking method for underwater targets tracking. In: MTS/IEEE OCEANS Conference. 2016, p. 1–5.

[17] Fernando R, Kilgard MJ. The CG tutorial: the definitive guide to programmable real-time graphics. Boston, MA, USA: Addison-Wesley Longman Publishing Co., Inc.; 2003.

[18] Urick RJ. Principles of underwater sound. Peninsula Publishing; 2013.

[19] Lee J. Digital image enhancement and noise filtering by use of local statistics. IEEE Transactions on Pattern Analysis and Machine Intelligence 1980;2(2):165–8.

[20] Papoulis A, Pillai S. Probability, random variables and stochastic processes. McGraw Hill; 2002.